Heliyon 10 (2024) e37546

Contents lists available at ScienceDirect

Heliyon

journal homepage: www.cell.com/heliyon

Research article

# Mechanism of Fuzheng Qudu prescription in the treatment of lung cancer based on network pharmacology and experimental validation

Binjie Su [a,1], Qiyuan Mao [b,1], Daorui Li [b], Yingyi Wu [a], Bo Wang [a,c,**], Xueqian Wang [b,*]

[a] Xinjiang Key Laboratory of Biological Resources and Genetic Engineering, College of Life Science and Technology, Xinjiang University, Urumqi 830017, China
[b] Department of Oncology, Guang'anmen Hospital, China Academy of Chinese Medical Sciences, Beijing 100053, China
[c] Experimental Animal Center, Xinjiang Medical University, Urumqi, 830017, Xinjiang China

ARTICLE INFO

*Keywords:*
Fuzheng Qudu prescription
Lung cancer
Immune function
Network pharmacology
Treatment

ABSTRACT

*Objective:* This research utilized network pharmacology to investigate the potential of Fuzheng Qudu prescription (FZQDP) in treating lung cancer (LC).

*Methods:* The components and their targets of FZQDP were analyzed for their relationship with LC-related targets using bioinformatics tools. Mouse Lewis lung carcinoma (LLC) cells were cultured *in vitro* and treated with FZQDP or cisplatin (DDP) before applying the MTT assay to determine FZQDP concentrations, and the IC50 value. According to the IC50 value, the effect of FZQDP on apoptosis and cell cycle was detected by flow cytometry. Mouse tumor growth was recorded using live animal imaging, and measurements of tumor and spleen weight were used to calculate the tumor inhibition rate and spleen index. The effects on mouse liver and kidneys were observed by analyzing levels of AST, ALT, BUN, and CRE in blood and hematoxylin and eosin (H & E) stained sections. Additionally, levels of IL-2, IL-10, IL-6, and IFN-γ in serum, along with the frequencies of $CD4^+$ and $CD8^+$ T cells in the spleen, were measured using Mouse multiple Cytokine Assay and flow cytometry, respectively.

*Results:* SRC, STAT3, MAPK3, and MAPK1 could be crucial targets of FZQDP in the treatment of LC. FZQDP demonstrated inhibition of LC cell proliferation and tumor growth, as well as enhancement of apoptosis and induction of G2 phase cell cycle arrest. Furthermore, FZQDP led to elevated levels of IL-2 and IFN-γ, increased frequencies of $CD4^+$ T cells and decreased levels of IL-6 and IL-10. Importantly, FZQDP did not exhibit any noticeable hepatotoxic or nephrotoxic effects in mice.

*Conclusion:* FZQDP may target multiple signaling pathways to treat LC. In a LC mouse model, FZQDP was found to inhibit tumor growth and improve immune function.

** Corresponding author. College of Life Science and Technology, Xinjiang University, 666 Shengli Road, Urumqi, Xinjiang 830017, China.
* Corresponding author. Oncology Department of Guang'anmen Hospital, China Academy of Chinese Medical Sciences, No.5 Bei xian ge, Xi Cheng District, Beijing, 100053, China.
*E-mail addresses:* wbxjhyj@aliyun.com (B. Wang), wxq791875354@126.com (X. Wang).
[1] Binjie Su and Qiyuan Mao contributed equally to this work.

https://doi.org/10.1016/j.heliyon.2024.e37546
Received 20 May 2024; Received in revised form 2 September 2024; Accepted 4 September 2024
Available online 6 September 2024

## 1. Introduction

Lung cancer (LC) is the second most prevalent cancer worldwide and the leading cause of cancer-related deaths [1]. In 2022, it was the most commonly diagnosed cancer, affecting approximately 2.5 million individuals and accounting for 12.4 % of global cancer cases [2]. Clinical observations have shown that many LC patients are diagnosed at an advanced stage, missing the optimal window for treatment [3,4]. Currently, surgery, radiotherapy, and chemotherapy are the primary treatment modalities for LC. However, surgery carries high risks, and radiotherapy and chemotherapy often result in significant side effects with limited patient survival time [5,6]. Traditional Chinese medicine (TCM) is extensively utilized in cancer treatment as a crucial adjuvant therapy. It is characterized by its multi-component and multi-target nature, minimal side effects, and holistic approach [7]. TCM has been shown to enhance immune function, suppress tumor growth, regulate the tumor microenvironment, and aid in preventing tumor metastasis and recurrence, particularly in breast cancer [8] and LC [9]. Additionally, TCM can mitigate the adverse effects of chemotherapy or radiotherapy, offering significant potential in supporting LC treatment [10,11]. Therefore, the search for suitable TCM options holds great importance in assisting LC treatment.

The Fuzheng Qudu prescription (FZQDP) is developed from the toxin theory of TCM for treating malignant tumors. It consists of five key TCM ingredients: *Astragalus membranaceus*, *Fritillaria thunbergii* Miq., turmeric, *Sophora flavescens* and *Salvia miltiorrhiza*. Numerous studies have demonstrated the anti-tumor properties of these ingredients, inducing tumor growth inhibition, induction of tumor cell apoptosis, and prevention of new blood vessel formation. For instance, *Astragalus* can restore the peritoneal immune environment and inhibit tumor blood vessel formation [12]; tanshinone IIA in *Salvia miltiorrhiza* can inhibit cell migration, tumor proliferation, and induce apoptosis and autophagy [13]; *Fritillaria thunbergii* Miq exhibits anti-inflammatory properties, induces apoptosis, and inhibits cell proliferation [14]; curcumin in turmeric is effective in treating colon cancer [15]; matrine in *Sophora flavescens* can induce cell cycle arrest, apoptosis, interfere with cancer metabolism, inhibit metastasis and angiogenesis, regulate aging, telomeres, tumor microenvironment and reduce cancer-related inflammation to inhibit colorectal cancer cell proliferation [15,16]. Studies have shown that FZQDP and formulations based on it, such as Fuzheng Huoxue Anticancer Formula, have shown promising therapeutic effects in liver and gastric cancers [17–20]. However, there is limited research on the efficacy of FZQDP on LC and its underlying mechanisms.

Network pharmacology, a multidisciplinary field merging biology and network informatics, has proven valuable in elucidating the mechanisms of action between TCM and diseases, as well as in the development of novel drugs [21]. TCM, known for its diverse components and targets [7], plays a crucial role in addressing complex diseases like cancer, which stem from mutations across multiple genes disrupting the biological network systems' equilibrium. Notably, network pharmacology analysis revealed that a decoction of four mild drugs contains 144 active chemical components and targets 897 potential targets for colorectal cancer [21]. Similarly, LC, characterized by mutations in genes like EGFR, P51, and DCCD, also disrupts the biological network system's balance [22–24]. Therefore, this study utilized network pharmacology analysis to investigate the potential targets and mechanisms of FZQDP in treating LC, supplemented by *in vitro* and *in vivo* validation to lay a theoretical foundation for further research on FZQDP in LC.

## 2. Materials and methods

*Ethics approval*

All animal experiments were conducted in compliance with national guidelines for animal experiments and approved by an animal care committee (The ethics committee of the Guang'anmen Hospital, China Academy of Chinese Medical Sciences, No. 2020-011-SQ).

### *2.1. Preparation of FZQDP extract*

The study utilized 675 g of *S. flavescens*, 900 g of raw *A. membranaceus*, 450 g of turmeric, 675 g of *F. thunbergii*, and 450 g of *S. miltiorrhiza,* all sourced from Guang 'anmen Hospital, China Academy of Chinese Medical Sciences. These ingredients were decocted, concentrated, freeze-dried, and crushed to produce 580.88 g of freeze-dried powder from the aqueous extract of FZQDP, resulting in a yield of 18.44 %. The freeze-dried powder was then mixed with a 70 % volume fraction methanol solution (20 mL), subjected to ultrasound extraction, and filtered to create the test solution. Additionally, individual quantities of *F. thunbergii*, turmeric, *S. flavescens*, raw *A. membranaceus,* and *S. miltiorrhiza* (5 g each) were combined with 20 mL of 70 % methanol solution, extracted via ultrasound for 30 min, filtered through a 0.22 μm microporous filter membrane, resulting in single drug solution which served as the reference solution.

### *2.2. Analysis of FZQDP extract by ultrahigh performance liquid chromatography-high-resolution mass spectrometry (UPLC-HRMS)*

The FZQDP extract was analyzed using an online Dionex Ultimate 3000 ultrahigh performance liquid chromatography system (Thermo Fisher, Waltham, MA, USA) with an ACQUITY UPLC HSS T3 column (100 × 2.1 mm, 1.8 μm, Waters, Milford, MA, USA) at a column temperature of 35 °C. The mobile phase A consisted of $H_2O$ + 0.1 % formic acid, while mobile phase B was acetonitrile +0.1 % formic acid (LC-MS solvent, Fisher Chemical, Waltham, MA, USA). Samples and controls were separated using the following gradient at a flow rate of 0.3 mL/min: 0–3 min, 98 % A; 3–25 min, 98-60 % A, 25–35 min, 60-5% A; 35–37 min, 5 % A. This system was coupled with an LTQ-Orbitrap velos Pro mass spectrometry (Thermo Scientific, Waltham, MA, USA) for LC-MS/MS analysis. The primary mass spectrometry of the test and reference solution was scanned in positive and negative modes of electrospray ionisation, with a capillary

temperature of 350 °C, capillary voltage of 35 V, and spray voltage of 3.5 kV under Fourier-transform mode, scanning a range of 100–1200 *m/z*. The secondary mass spectrometry was performed by data-dependent scanning. Mass spectrometry data were collected and analyzed using Xcalibur software (OPTON-30965, Thermo Fisher) [25].

### 2.3. Active ingredient screening and target prediction of FZQDP

By leveraging TCM pharmacology databases such as TCMSP and TCMIP, along with metabolomic analysis, the primary components of FZQDP (*A. membranaceus*, *S. miltiorrhiza*, turmeric, *S. flavescens*, and *F. thunbergii)* were systematically gathered and their targets were scrutinized using the Swiss Target Prediction website database. The key parameters for drug screening, namely oral bioavailability (OB) and drug-like properties (DL), were defined as OB $\geq$ 30 % and DL $\geq$ 0.18. Subsequently, targets corresponding to the target proteins were searched from the Unitprot database (http://www.Uniport.org/), and targets for the constituents of FZQDP were extracted. The PubChem database (https://pubchem.ncbi.nlm.nih.gov/search/) was then accessed to retrieve the optimized molecular linear input standard formula SMILES for the active ingredients of *A. membranaceus*, *S. miltiorrhiza*, turmeric, *S. flavescens*, and *F. thunbergii*-related targets of FZQDP.

The Swiss Target Prediction database (http://www.Swisstargetprediction.ch/), which operates on reverse molecular docking technology, was employed to accurately predict biologically active targets. Utilizing joint detection for prediction and analysis based on the 2D and 3D similarity of identified ligands, the database was accessed, the species "Homosapiens" was selected, and the SMILES formula corresponding to the targets was inputted [26]. Following the screening, the potential targets of the active ingredients in *A. membranaceus*, *S. miltiorrhiza*, turmeric, *S. flavescens*, and *F. thunbergii* of FZQDP on human body were determined [26].

### 2.4. Prediction of LC-related targets

The keyword "lung cancer" was imported into the DisGeNET database (https://www.disgenet.org/), GeneCards database (https://www.genecards.org/), and OMIM database (https://www.omim.org/) for search, with duplicates removed. Common targets for FZQDP and LC were identified using Venny 2.1.0 online tool (https://bioinfogp.cnb.csic.es/tools/venny/). A drug-active ingredient-disease-common target relationship network diagram was then created using Cytoscape 3.7.2 software. Key targets were analyzed using the Network Analyzer function, where the size of network nodes represented the degree value [27,28].

### 2.5. Protein-protein interaction (PPI) network establishment

By importing the common targets of FZQDP and LC into the STRING platform, a PPI network was generated. The protein type was specified as "Homo sapiens" with a minimum interaction score of 0.700. Subsequently, the PPI data was imported into Cytoscape 3.7.2 software and filtered using the molecular complex detection (MCODE) plugin. Key targets were identified based on their "Degree" score for visualization purposes [25].

### 2.6. Gene Ontology (GO) analysis and Kyoto Encyclopedia of Genes and Genomes (KEGG) analysis

The common targets identified after STRING treatment were uploaded to the Metscape database for GO enrichment analysis and KEGG pathway analysis. Using a screening condition of P value $\leq$ 0.05, significantly expressed genes were identified within the GO entries. To gain a deeper understanding of the therapeutic role of *A. membranaceus*, *S. miltiorrhiza*, turmeric, *S. flavescens*, and *F. thunbergii* of FZQDP for treating LC, the gene analysis tool DAVID was utilized to analyze the core targets identified by the PPI network and the key biological pathways. The overlapping genes were then inputted into the DAVID database, with the species set as "H.sapiens". The core targets for LC treatment underwent GO enrichment analysis [biological processes (BP), molecular functions (MF), cellular components (CC)] and KEGG pathway analysis. The enrichment results were filtered and visualized based on P-value, and the corresponding bubble plot was generated using the microbiological information platform (https://www.bioinformatics.com.cn/) [21].

### 2.7. Cell culture and treatment

Lewis lung carcinoma (LLC) cells were sourced from the American Type Culture Collection (ATCC, Manassas, VA, USA). and cultured in Dulbecco's Modified Eagle Medium (DMEM) (10564011, GIBCO, NY, USA) supplemented with 1 % penicillin/streptomycin, 5.5 mM glucose, and 10 % fetal bovine serum (10099, GIBCO, NY, USA). Subsequently, the cells were cultured in a controlled environment of 5 % carbon dioxide and 95 % humidified air at 37.0 °C.

### 2.8. MTT assay

LLC cells in the logarithmic growth phase were harvested and adjusted to a cell density of 5 $\times$ 103 cells/mL post-trypsin digestion. These cells were then plated in 96-well plates at a volume of 100 μL per well. Following treatment with varying concentrations of FZQDP extract (0, 10, 100, 500, 1000, 2500, 5000, 7500, 10000 μg/mL) for 24 h, the culture medium was removed, and MTT-containing medium was added for 4 h. Subsequently, the medium was aspirated, and dimethyl sulfoxide (DMSO) (150 μL/well) was added and mixed thoroughly for 10 min. The optical density (OD) of each well was measured at 490 nm using a microplate reader

(Varioskan™; Thermo Scientific, Rockford, IL, USA) to determine the half-maximal inhibitory concentration (IC50). Triplicate independent experiments were repeated.

### 2.9. Cell grouping

Following the MTT assay, the IC50 value of FZQDP was determined to be 3243 μg/mL. Subsequently, the cells were categorized into the following groups for treatment: (1) Blank group, where cells were exposed to 10 mM PBS buffer (P3744, Sigama-Aldrich) for 24 h; (2) FZQDP group, where cells were treated with 3200 μg/mL FZQDP for 24 h; (3) DDP group, where cells were treated with 66 μM DDP for 24 h, serving as a positive control of FZQDP.

### 2.10. Cell cycle and apoptosis experiments

Cells were collected in 60 mm culture dishes and washed with phosphate-buffered saline (PBS). Subsequently, they were resuspended in pre-chilled 70 % ethanol and fixed at −20 °C overnight. Following removal of ethanol residue by centrifugation and another wash with PBS, the cells were stained with propidium iodide (PI) (ST1569, Beyotime, Shanghai, China) and then incubated at 4 °C in the dark for 30 min. Cell cycle phase distribution was evaluated using flow cytometry (Becton Dickinson, San Jose, CA, US). Triplicate independent experiments were repeated.

Cells and culture medium from each well in the 6-well plate were collected and centrifuged to remove the supernatant. The cells were then resuspended in a PBS cell suspension for counting. Subsequently, after centrifugation to eliminate the supernatant, $1 \times 10^5$ cells were resuspended in 195 μL of Annexin V-FITC binding buffer. Subsequently, 5 μL Annexin V-FITC (C1062S, Beyotime) was introduced and thoroughly mixed with the cells, followed by the addition of 10 μL the PI staining solution. The resulting mixture was incubated in darkness for 15 min prior to apoptosis analysis using flow cytometry. Triplicate independent experiments were repeated.

### 2.11. Mouse and establishment of tumor model

Eighteen male C57BL/6J mice (4–6 weeks old, average weight 20 g) were obtained from Vital River [SYXK (Beijing), 2016-0011, Beijing, China] and housed individually at 20–26 °C with ad libitum access to food and water and a relative humidity of 50%–60 %. The luciferase-labeled Lewis cell line was obtained from the Cancer Laboratory of Guang'anmen Hospital, China Academy of Chinese Medical Sciences (Beijing, China).

LLC cells labeled with luciferase ($5 \times 10^5$ cells) were injected subcutaneously into the right armpit of mice at a dose of 0.2 mL of cell suspension per mouse. The day of injection was designated as day 0, and on the following day, the mice were randomly assigned to the Model, FZQDP and cisplatin (DDP) groups. Starting from the 2nd day after injection, the FZQDP group received a dose of 0.2 mL FZQDP (0.2 g/mL) by gavage and the drug concentration was calculated according to the dose group in the literature [17]. The mouse dose was calculated based on the maximum human dose of each component in the Pharmacopoeia of the People 's Republic of China, considering the conversion factor between humans and mice (mouse dose = 9.1 × human clinical dose for a 60 kg human). The drug dosage administered to the mice was within the safe range. For instance, the maximum dose of one component of *Sophora flavescens* in mice was calculated as 9.1 × human clinical dose (60 kg human with 9 g *Sophora flavescens*) [29]. The FZQDP group received the treatment once daily for 20 consecutive days, while the Model and DDP groups were given 0.2 mL of PBS by gavage. Circular-like protrusions were observed and palpated subcutaneously in the armpits of mice on the 7th day, indicating successful modeling. On the day of successful modeling, the DDP group received 0.2 mL purified water by gavage, and simultaneous intraperitoneal infusion of DDP (Qilu Pharmaceutical, National medicine permission number: H20073652, Hainan, China) at a dose of 5 mg/kg, 3 times a week, for 2 consecutive weeks (6 infusions) as a positive control. The other groups were injected with the same volume of PBS. On the 21st day, all animals were euthanized by intraperitoneal injection of 100 mg/kg pentobarbital sodium to collect blood, spleens, and tumors. Throughout the study, the weight changes of the mice on days 0, 7, 14, and 21 were monitored.

### 2.12. In vivo bioluminescent imaging

Following weighing on the day of imaging, the mice received intraperitoneal injections of D-Luciferin potassium salt (PerkinElmer, Waltham, MA, USA) at a dose of 0.2 mL/20 g. Imaging was conducted using an *in vivo* fluorescence imaging system from Caliper Life Sciences (Hopkinton, MA, USA), and analysis was performed using Spectrum Living Image 4.0 software (Caliper Life Sciences).

### 2.13. Pathological examination (H&E staining)

The liver and kidney tissues of mice were fixed with 4 % paraformaldehyde for 24 h, dehydrated, embedded in paraffin, and cut into 4 μm thick sections. Subsequently, the sections underwent dewaxing with xylene, rehydrated with gradient alcohol, and stained with hematoxylin for 5 min. Following a 5-min wash with tap water, the slices were briefly immersed in a 1 % hydrochloric acid alcohol differentiation solution, followed by restaining in a 0.5 % eosin solution for 5 min. The sections then underwent conventional dehydration, clarification, and sealing with neutral resin before being observed under an optical microscope.

The degree of liver injury is assessed using the semi-quantitative Knodell liver score, which evaluates four inflammatory indicators independently. These include necrosis around the portal area (0–10 points), lobular degeneration and focal necrosis (0–4 points), volume of inflammation in the portal area (0–4 points), and degree of liver fibrosis (0–4 points) [30]. On the other hand, renal injury

histopathological changes are evaluated based on the percentage of tubular damage/impairment, which includes tubular loosening, dilation, destruction, and cast formation. Tissue damages were scored on a scale of 0–4, with each number corresponding to a specific range of injured/damaged renal tubules. Specifically, 0 % for 0, less than 25 % for 1, 26%–50 % for 2, 51%–75 % for 3, and equal to or more than 76 % for 4 [31]. To ensure accuracy, ten fields of view are randomly selected for each slice.

### 2.14. Determination of tumor inhibition rate and spleen index

After 24 h of administration on the 21st day, the mice were euthanized. Tumors and spleens were then collected, weighed, and photographed. Subsequently, the tumor inhibition rate and spleen index were calculated. The tumor inhibition rate was determined using the formula: (average tumor weight in the model group - average tumor weight in the treatment group) divided by average tumor weight in the model group, multiplied by 100 %. The spleen index was calculated as spleen weight divided by mouse weight, multiplied by 100 %.

### 2.15. Mouse multiple cytokine assay

Following anesthesia of the mice, blood samples were collected by removing the eyeballs. The samples were then incubated at room temperature for 30 min and subsequently centrifuged at 3500 rpm at 4 °C for 10 min to obtain serum, which was stored at −80 °C. Subsequently, the levels of interleukin (IL)-2, interferon (IFN)-γ, IL-10 and IL-6 were quantified using the Mouse Bio-Plex Pro Assays Mouse Multifactor kits (M60009RDPD, Bio-rad, Hercules, CA, USA). Serum samples were diluted 1:2 in assay diluent while serially diluting standards. Samples were added to plates containing magnetic antibody-coupled beads for each analyte and incubated with rotation at room temperature for 30 min (300 rpm). The plate was then washed with Bio-Plex Wash Buffer, and the secondary antibody was added to the plate and incubated with rotation at room temperature (300 rpm) for 30 min, followed by additional washes. Streptavidin-phycoerythrin was added to the plate and incubated for 10 min at room temperature in the dark with rotation (300 rpm). Assay buffer was added to each well and plates were analyzed on the Bio-Plex® 200 system. A reference curve was established based on the fluorescence intensity of the standard sample, and the cytokine concentration in the sample was calculated. Triplicate independent experiments were repeated.

### 2.16. Blood biochemical assessment

Serum samples were thawed from −80 °C to 4 °C before detecting aminotransferase (AST), alanine aminotransferase (ALT), urea nitrogen (BUN), and creatinine (CRE) using kits provided by Nanjing Jiancheng Bioengineering Institute (Nanjing, China). The operating procedures recommended by the institute were followed during the detection process. Triplicate independent experiments were repeated.

### 2.17. Flow cytometry

Twenty-four hours post final dose administration, mouse spleens were placed into 6-well plates comprising pre-chilled phosphate buffered saline (PBS; 1 mL). Following homogenization, cells were filtered using a 200-mesh sieve, lysed for 5 min on ice with 1 mL hemolysin in the dark, and centrifuged for 5 min at 1200 g. The resulting pellet was resuspended in PBS, a process repeated twice. Subsequently, each splenocyte suspension (100 μL) was stained with FITC Rat Anti-Mouse CD8a (561966, BD Biosciences, San Jose, CA, USA) and APC-CyTM 7 Rat Anti-Mouse CD4 (565650, BD Biosciences) in the dark for 25 min. The samples were then rinsed twice with pre-cooled PBS containing bovine serum albumin before being analyzed by flow cytometer. Data analysis was performed using FlowJo X 10.0.7r2 (Becton Dickinson, Ashland, OR, USA)

### 2.18. Statistical analysis

The measured data were presented as mean ± standard deviation (SD). Group comparisons were conducted using one-way analysis of variance (ANOVA), followed by Tukey's test. Repeated measures analysis of variance was employed for data collected at multiple time points. Nonparametric tests were utilized for data that did not follow a normal distribution. A significance level of $P < 0.05$ was considered statistically significant. Statistical analysis was carried out using GraphPad Prism 8.01 software (GraphPad, San Diego, CA, USA) and SPSS 24.0 (IBM Corp. Armonk, NY, USA).

## 3. Results

### 3.1. Analysis of FZQDP components and their therapeutic targets for LC

The composition of FZQDP was determined using the UPLC-HRMS method. Through experimental data and literature analysis, a total of 100 compounds were identified and inferred, including flavonoids, flavonoid glycosides, alkaloids, quinones, saponins, phenolic acids, and other categories (Supplementary Table 1). Specifically, 28 compounds were from *S. flavescens*, 26 from *A. membranaceus*, 20 from *S. miltiorrhiza*, 15 from *F. thunbergii*, and 11 from turmeric (Fig. 1A). Subsequently, the active ingredients and targets of TCM were explored using the TCMSP database, revealing an overlap of active components and targets of TCM, as depicted in

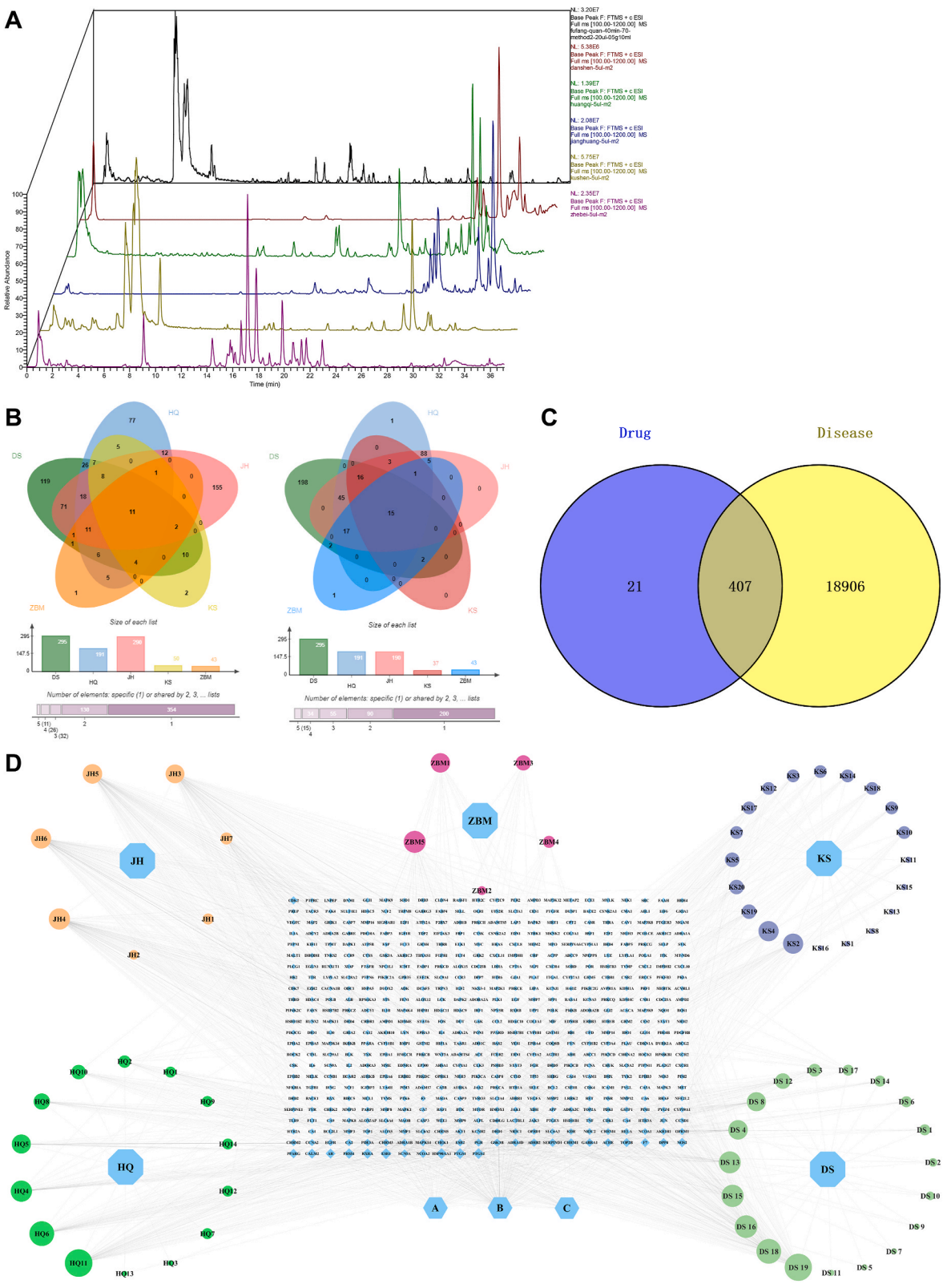


**Fig. 1.** Prediction of FZQDP components and their therapeutic targets for lung cancer. A: UPLC-HRMS method was used to detect the components of FZQDP; B: Venn diagrams of multiple drug components and corresponding targets; C: Venn diagrams of FZQDP and lung cancer; D: Network diagram of drug-active ingredient disease common target relationship drug-active ingredient-disease-common target relationship.

Fig. 1B. A total of 19313 targets were retrieved from the DisGeNET, GeneCards, and OMIM databases for LC. By employing Venny online mapping, 407 common targets of FZQDP and LC were identified (Fig. 1C). A network diagram illustrating the drug-active ingredient-disease-common target relationship was generated using Cytoscape (Fig. 1D), which comprised 466 nodes and 1403 edges. Network analysis indicated a centrality of 0.07, a heterogeneity of 1, and an average CC of 0.33, suggesting varying importance of nodes within the network. The average degree of the network was 10.76, with 103 component nodes exceeding this value. Notably, the highest degree was observed for *Sophora flavescens* nodes among the five TCMs, connecting to 173 target nodes. The interaction between these components and targets signifies that FZQDP exerts its effects on multiple targets through various components in the treatment of LC.

### 3.2. Identification of key targets and establishment of PPI network

To identify key targets, common targets were inputted into the STRING platform with a confidence level of 0.700 to establish a PPI network (Fig. 2A). The results were then visualized using Cytoscape, with the "Degree" score utilized as the criterion for screening key targets (Fig. 2B). The network consisted of 227 nodes and 1326 edges. Analysis of the network revealed an average node degree of 11.06, and 104 targets surpassing this average, highlighting the top 10 nodes. The findings suggested that nonreceptor tyrosine kinase

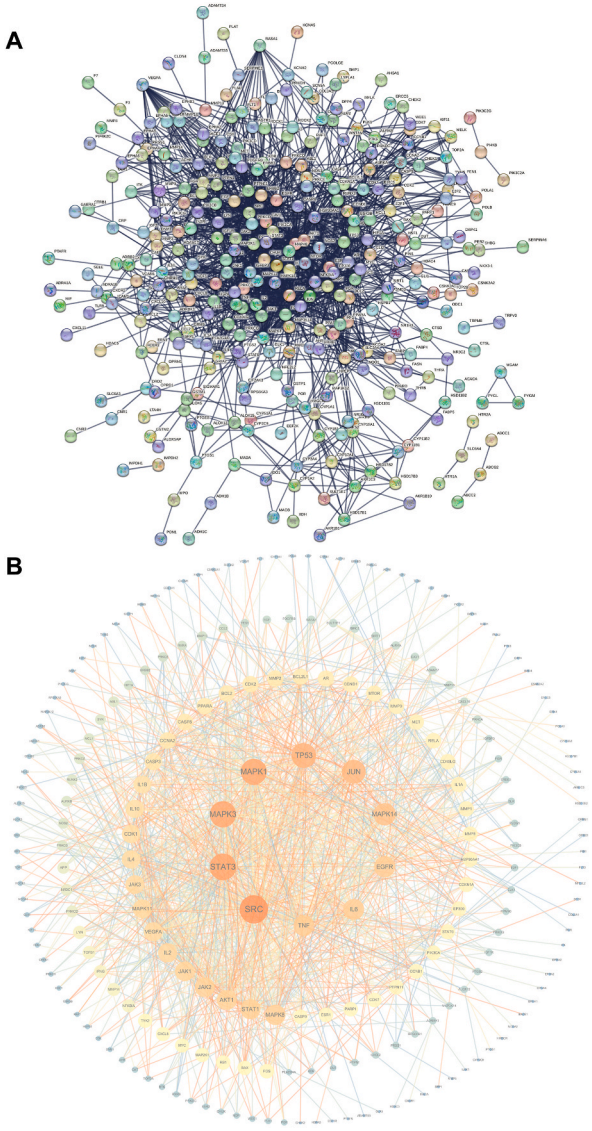


**Fig. 2.** Network analysis of potential targets of components in FZQDP. A: PPI network interaction diagram of common targets between FZQDP and lung cancer; B: Screening of key targets of FZQDP and lung cancer. The size and color depth of nodes were proportional to their Degree. (For interpretation of the references to color in this figure legend, the reader is referred to the Web version of this article.)

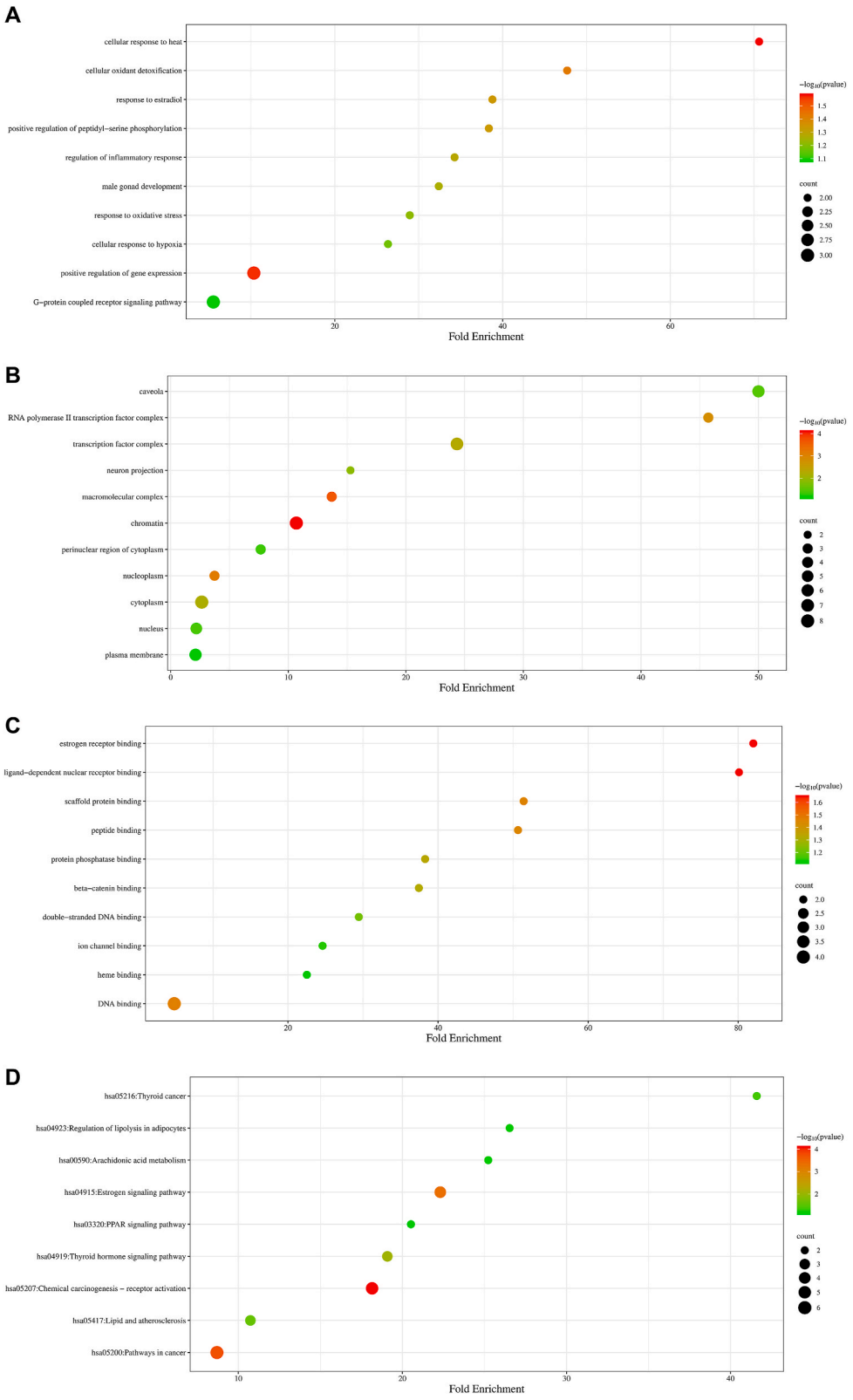


**Fig. 3.** GO enrichment analysis and KEGG enrichment analysis. A: BP bubble chart; B: CC bubble chart; C: MF bubble chart; D: KEGG enrichment analysis.

(SRC), signal transducer and activator of transcription 3 (STAT3), mitogen activated protein kinase (MAPK) 3, MAPK1, tumor protein p53 (TP53), Jun proto-oncogene (JUN), MAPK14, epidermal growth factor receptor (EGFR), IL-6, and tumor necrosis factor (TNF) may be pivotal targets of FZQDP for treating LC.

### 3.3. GO and KEGG enrichment analyses of potential targets

To elucidate the potential functions of common targets, the Metscape database was used for GO enrichment analysis and KEGG enrichment analysis. The GO enrichment analysis yielded 3 categories: BP, CC, and MF. Bubble diagrams were used to represent the top 10 items of P value in BP and MF, as well as the top 11 items of P value in CC. The findings of the GO enrichment analysis revealed that the targets of FZQDP in treating LC primarily exerted their effects through BP such as cellular response to heat, positive regulation of gene expression, and cellular oxidant detoxification (Fig. 3A). In terms of cellular components, the targets were associated with caveola, chromatin, RNA polymerase II transcription factor complex, and macromolecular complexes (Fig. 3B). MFs of the targets included DNA binding, estrogen receptor binding, ligand-dependent nuclear receptor binding, and scaffold protein binding (Fig. 3C). KEGG enrichment analysis identified the top 9 target enrichment pathways based on P-value (Fig. 3D), with pathways in cancer, chemical carcinogenesis-receptor activator, and estrogen signaling pathways being the most enriched. The cancer pathways with the highest number of enriched targets were further analyzed. As illustrated in Fig. 4, the yellow-labeled targets represented the targets of FZQDP involved in cancer, regulation, suggesting its role in modulating multiple cancer pathways.

### 3.4. FZQDP suppressed LLC cell viability and induced cell apoptosis and G2 phase arrest

Based on network pharmacology analysis predictions, the impact of FZQDP on LLC cells was investigated through *in vitro* experiments. MTT results indicated a significant decrease in cell viability at a concentration of 100 μg/mL of FZQDP, with an IC50 value of 3243 μg/mL for LLC cells. Subsequent experiments utilized a concentration of 3200 μg/mL of FZQDP, based on the IC50 value (Fig. 5A, all $P < 0.01$). Flow cytometry analysis showed a decrease in S phase cells and an increase in G2 phase cells in the FZQDP group compared to the Blank group, indicating G2 phase arrest induced by FZQDP, which was enhanced after DDP treatment (Fig. 5B, all $P < 0.01$). Additionally, cell apoptosis was promoted in cells treated with FZQDP or DDP compared to the control group (all $P < 0.001$), as shown in Fig. 5C. Overall, FZQDP demonstrated the ability to inhibit LLC cell viability, induce cell apoptosis, and cause G2 phase arrest.

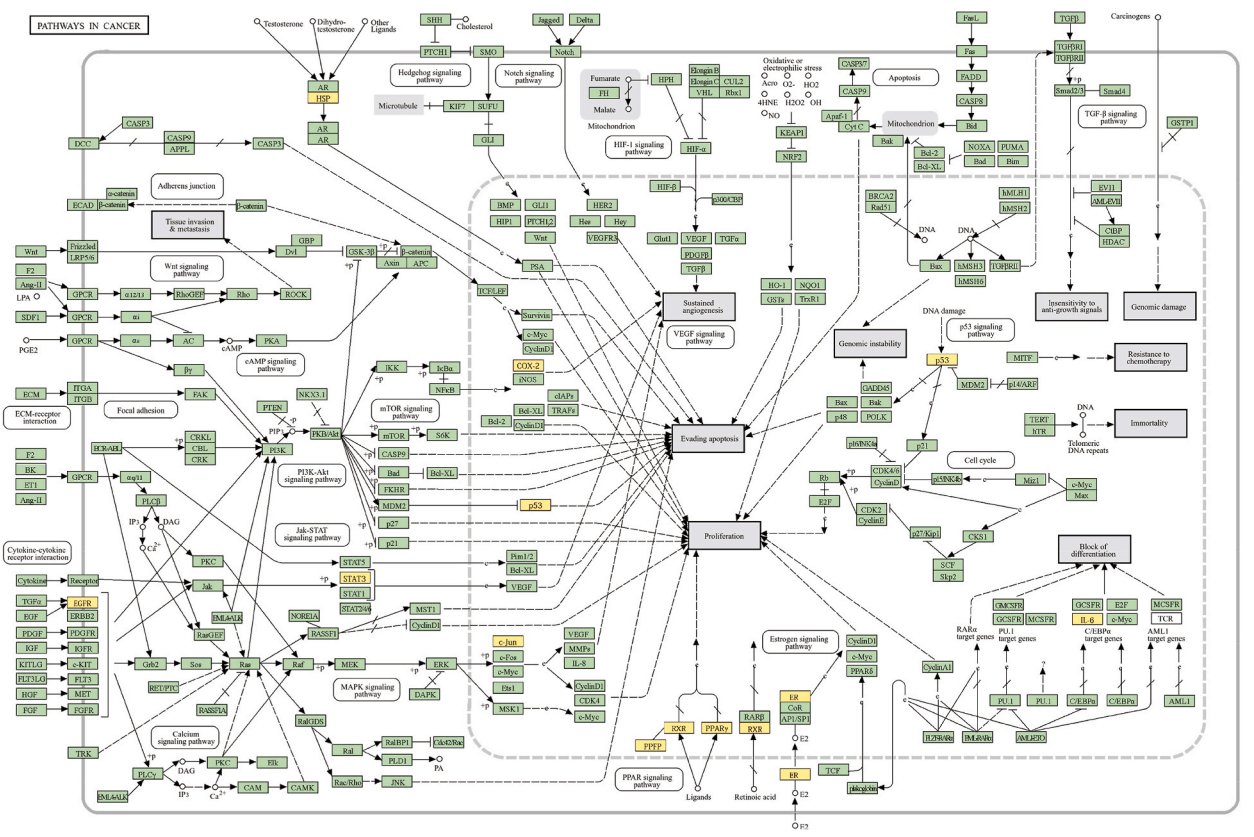


**Fig. 4.** Pathway map for KEGG enrichment analysis of cancer-related pathways.

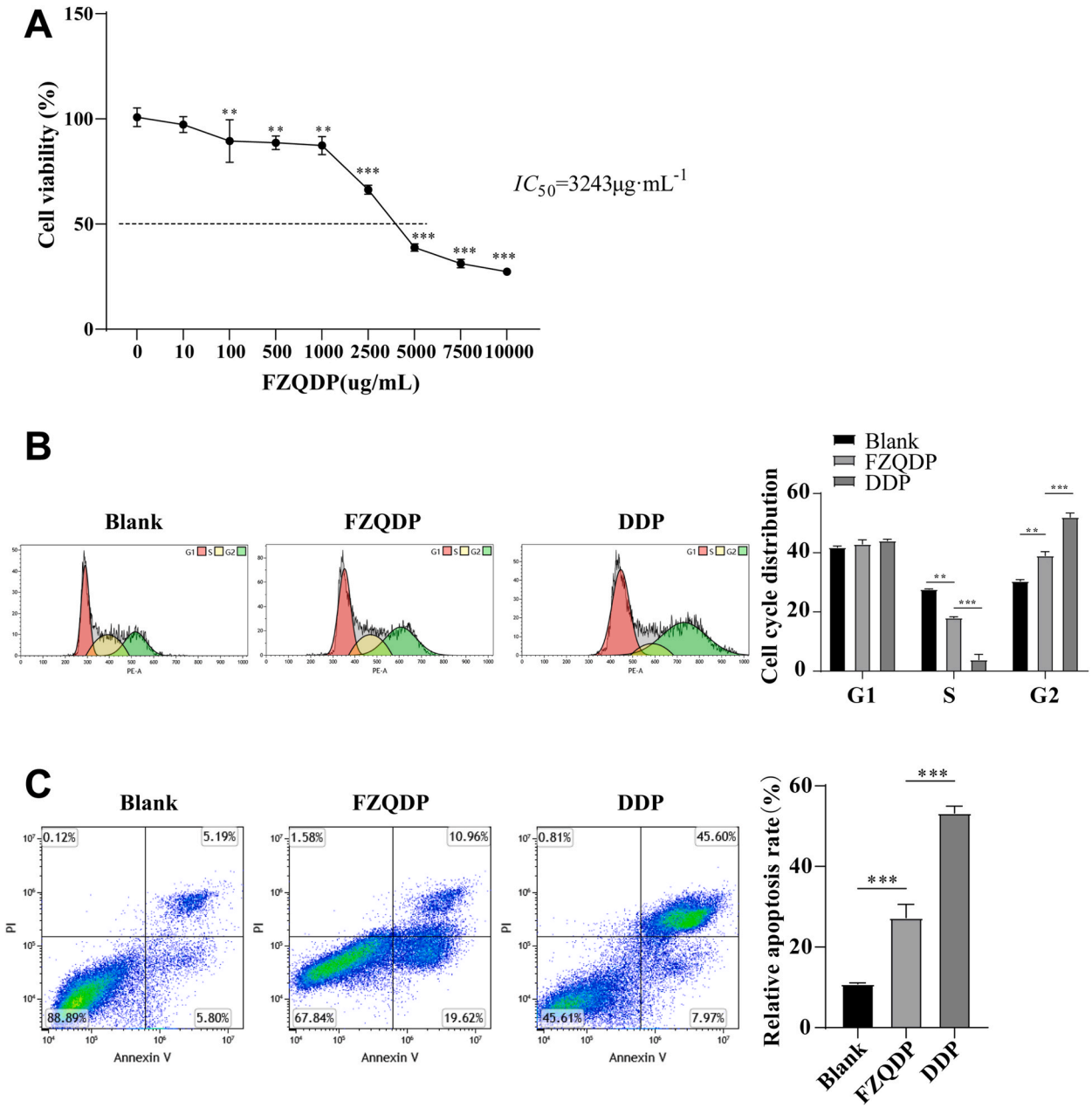


**Fig. 5.** FZQDP inhibited LLC cell activity and induced apoptosis and G2 phase arrest. A: MTT for cell activity and IC50 value, compared with Blank group; B: Flow cytometry for cell cycle; C: Flow cytometry for apoptosis. Data were expressed as mean ± standard deviation. Comparisons between multiple groups were performed by one-way ANOVA, and post hoc tests were performed by Tukey's multiple comparisons test. $^{**}P < 0.01$, $^{***}P < 0.001$.

### 3.5. *FZQDP suppressed the tumor growth in mouse LC model*

To further investigate the inhibitory effect of FZQDP on LC through *in vivo* experiments, a Lewis LC tumor model was established in C57BL/6J mice. The weight changes of the mice were monitored on days 0, 7, 14, and 21. Results showed that there were no significant differences in weight between the FZQDP and Model groups (Fig. 6A, $P > 0.05$), whereas the DDP group experienced notable weight loss (Fig. 6A, $P < 0.05$). Tumor growth status was assessed through live animal imaging, indicating that both FZQDP and DDP treatment suppressed tumor growth in comparison to the Model group. However, the tumor inhibition effect of DDP was more pronounced (Fig. 6B). Subsequent analysis of tumor weight post-euthanasia demonstrated a significant reduction after FZQDP and DDP treatment (Fig. 6C, $P < 0.05$). In conclusion, both FZQDP and DDP were effective in suppressing the growth of Lewis LC tumors in C57BL/6J mice, with FZQDP showing a lesser impact on the mice's body weight compared to DDP.

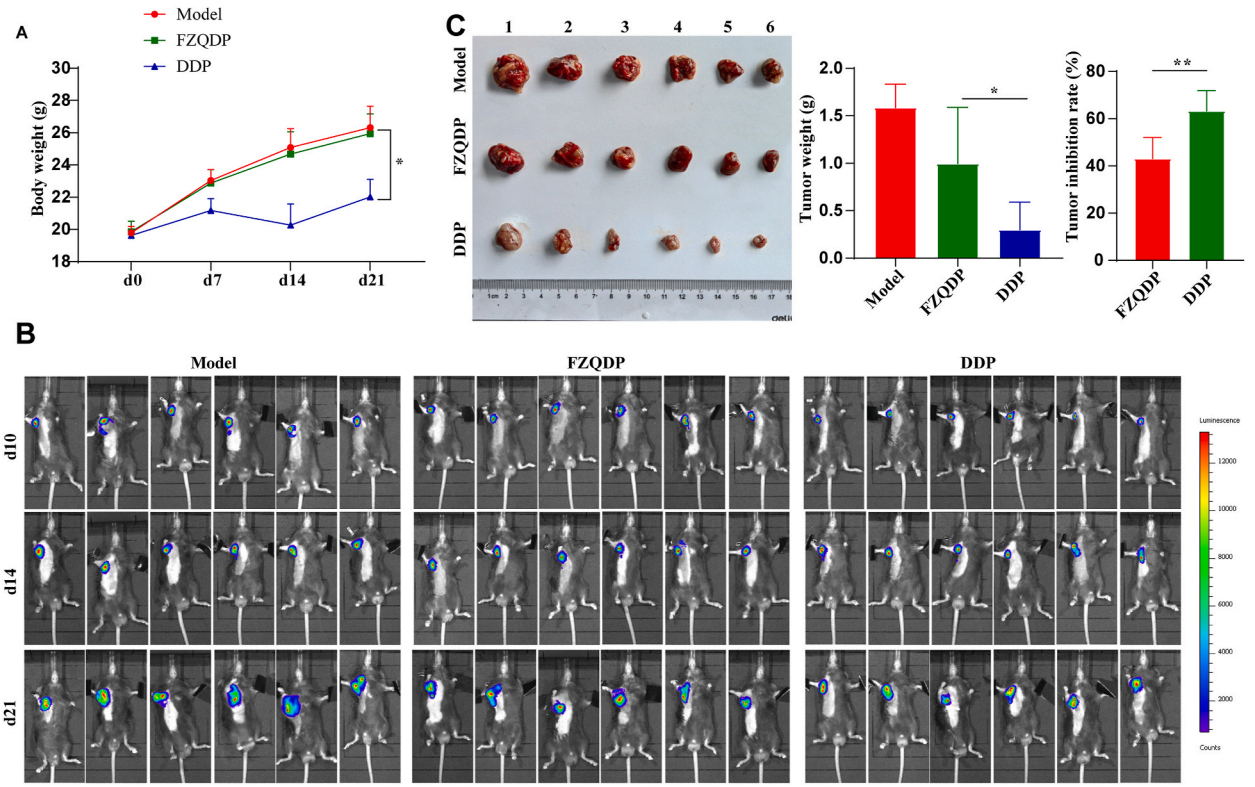


**Fig. 6.** FZQDP suppressed the growth of Lewis lung cancer xenograft tumor in C57BL/6 mice. A: Mouse body weight; B: Live animal imaging; C: The tumor weight and tumor inhibition rate of mice. N = 6. Data were expressed as mean ± standard deviation. One-way ANOVA was for comparisons among groups, followed by Tukey's test. *$P$ <0.05, **$P$ < 0.01.

### 3.6. FZQDP enhanced the immune function of tumor-bearing mouse

The study further examined the impact of FZQDP on the immune function of C57BL/6J mice. Spleens were weighed and spleen indexes were calculated. Compared to the Model group, the FZQDP group did not show a significant difference in spleen index (Fig. 7A, $P > 0.05$), while the DDP group exhibited a significant decline (Fig. 7A, $P < 0.05$), indicating that FZQDP did not cause notable damage to the mice's spleen, unlike DDP. Subsequently, the levels of IL-2, IFN-γ, IL-6 and IL-10 in serum were assessed. Both the FZQDP and DDP groups showed increased levels of IL-2 and IFN-γ compared to the Model group, with a notable decrease in IL-6 and IL-10 levels in the FZQDP group and a significant increase in the DDP group (Fig. 7B, all $P < 0.05$). Flow cytometry analysis of T cell subsets in mouse spleen revealed that FZQDP treatment led to an increase in the percentage of $CD4^+$ T cells and $CD4^+/CD8^+$ ratio, along with a decrease in $CD8^+$ T cells. Conversely, DDP treatment resulted in a decrease in $CD4^+$ T cells and $CD4^+/CD8^+$ ratio, coupled with an increase in $CD8^+$ T cells(Fig. 7C, all $P < 0.05$). In summary, FZQDP was found to enhance the immune function of mice with minimal impact on immune organs, while DDP had detrimental effects on immune organs and immune function.

### 3.7. Toxicity observation of FZQDP

The experiment involved monitoring the body weight and overall appearance of each mouse throughout. There was no significant weight loss observed after the FZQDP treatment (Fig. 6A, $P > 0.05$). Examination of H & E staining sections of the liver and kidney revealed that the level of liver and kidney damage in the FZQDP group and the model group was similar, but notably lower than that in the DDP group (Fig. 8A). Kidney sections from the DDP group showed signs of chronic inflammatory cell infiltration, necrosis of renal tubular epithelial cells, increased cortical tubular epithelial cell volume, cytoplasmic loosening, and numerous vacuoles; liver sections exhibited lysis and disappearance of necrotic hepatocytes, liver cell necrosis, and local inflammatory cell infiltration (Fig. 8A).

The blood biochemical indicators measured in the study (Fig. 8B) revealed that the ALT, AST, BUN, and CRE levels of the FZQDF group did not differ significantly from the model group. In contrast, the ALT, AST, BUN, and CRE levels in the DDP group were notably higher than those in the FZQDF group, displaying significant differences. Specifically, the ALT, BUN, and CRE levels in the DDP group were elevated compared to the model group, with no significant difference observed in AST levels. Notably, the AST level in the FZQDF group was significantly lower than that in the DDP group, suggesting lower liver and kidney toxicity in the FZQDF group compared to the DDP group.

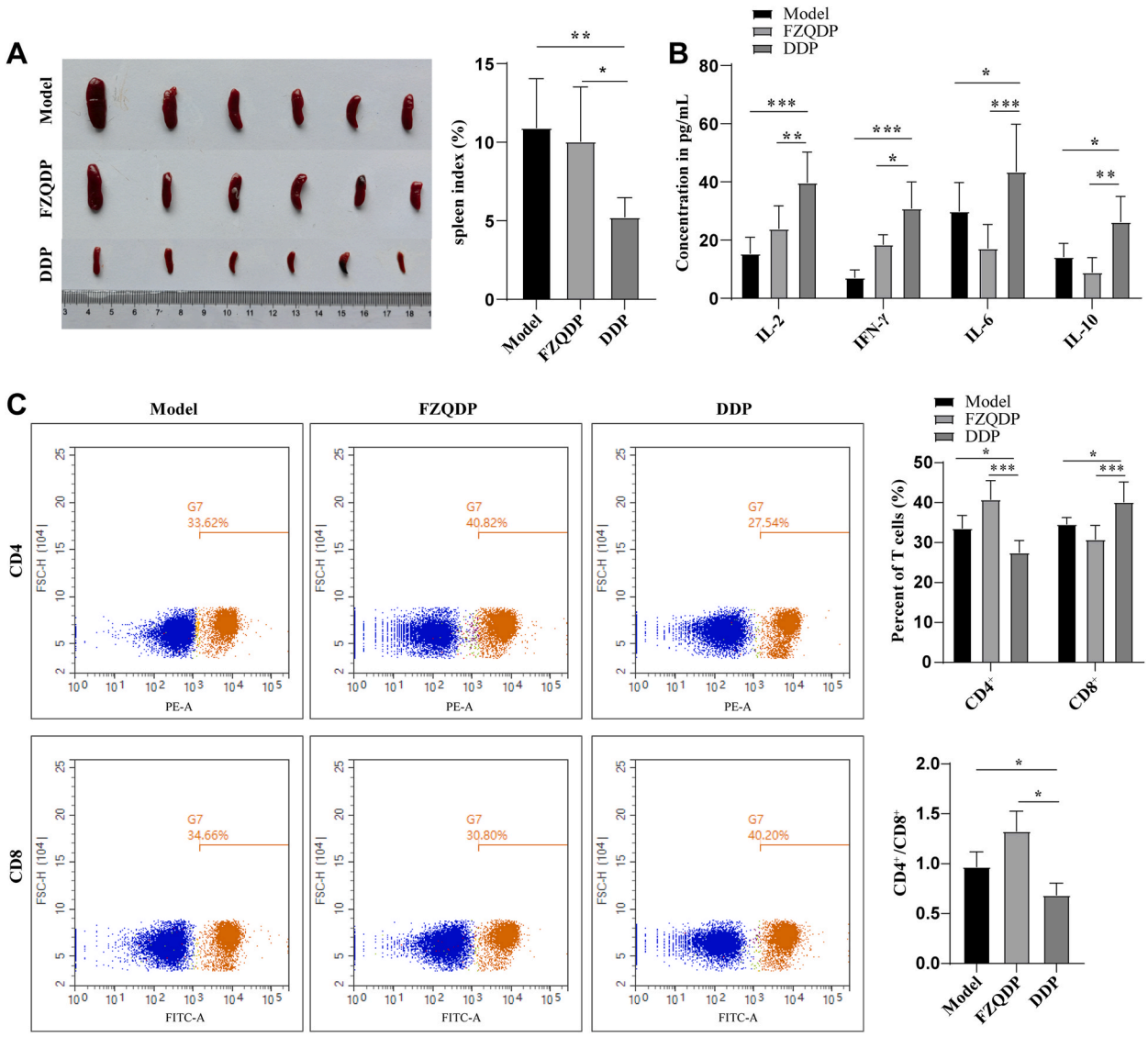


**Fig. 7.** The effect of FZQDP on the immune function of C57BL/6 mice. A: The spleen weight and spleen index of mice; B: The levels of IL-2, IFN-γ, IL-6 and IL-10 in serum; C: The frequency of $CD4^+$ and $CD8^+$ T cells and the ratio of $CD4^+/CD8^+$ in the spleen. N = 6. Data were expressed as mean ± standard deviation. One-way ANOVA was for multiple group comparisons, and Tukey's test was for post hoc testing. *$P$ <0.05, **$P$ < 0.01, *** $P$ < 0.001.

## 4. Discussion

LC is a malignant tumor known for its low survivability, rapid proliferation rate, metastatic potential, and high mortality rates [4]. It is a complex disease with numerous genetic alterations [32]. Despite advancements in understanding its development, risks, treatment options, and immune regulation, LC remains a leading cause of cancer-related deaths [2,33]. Standard therapies such as radiotherapy, immunotherapy, targeted therapy, chemotherapy and surgery have improved the prognosis for LC patients, with immunotherapy showing promising results [5]. However, radiotherapy and chemotherapy often lead to severe toxicity, reducing survival rates [5,6]. TCM has shown advantages in extending survival and enhancing quality of life for advanced LC patients, but its overall impact in the field of LC is not well-understood [34]. This study focused on investigating the key targets of FZQDP in LC treatment to elucidate its specific role, and subsequently confirmed its anti-tumor effects and safety *in vitro* and *in vivo*. Network pharmacology analysis revealed potential targets (STAT3, SRC, MAPK1, MAPK3, JUN, TP53, EGFR, MAPK14, TNF, and IL-6) and related pathways (PPAR, AMPK and p53) of FZQDP in LC treatment. *In vitro* experiments demonstrated that FZQDP effectively inhibited the growth of LC cells by inducing apoptosis and cell cycle arrest. In a mouse model of Lewis LC xenograft tumors, FZQDP significantly suppressed tumor growth and boosted immune function in mice, with no apparent side effect.

TCM has been a well-established medical approach, included in China's basic medical insurance plans for the treatment of LC [35].

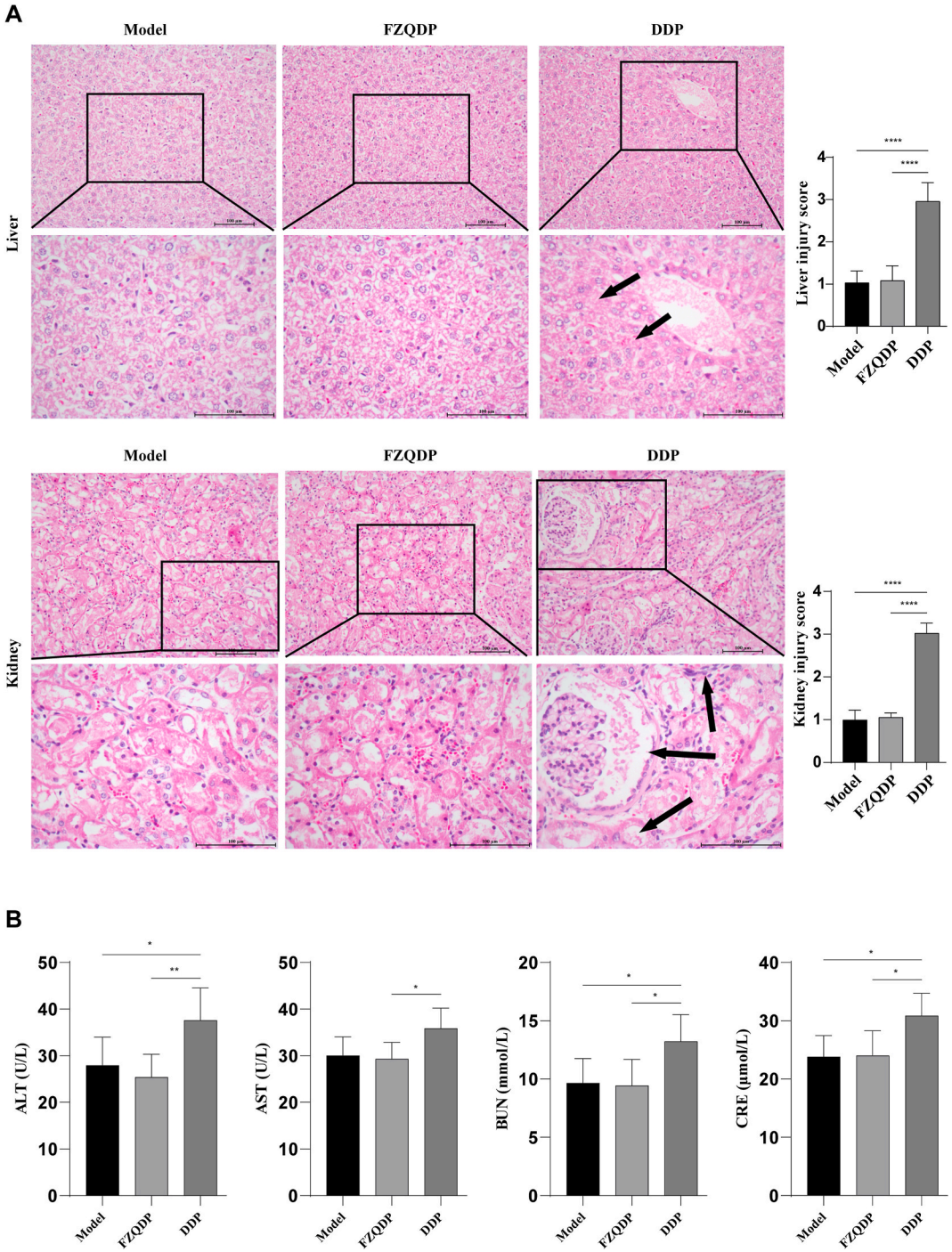


**Fig. 8.** A: HE staining was performed to analyze pathological damage in mouse liver and kidney. The black arrow indicates the site of the observed damage. B: Mouse blood biochemical assessment included measurements of AST, ALT, BUN, and CRE levels. Data were expressed as mean ± standard deviation. One-way ANOVA was for comparisons among groups, followed by Tukey's test. $^{*}P < 0.05$, $^{**}P < 0.01$, $^{****}P < 0.0001$.

The key ingredients of FZQDP were initially identified *as Astragalus membranaceus*, *Salvia miltiorrhiza*, turmeric, *Sophora flavescens* and *Fritillaria thunbergii* Miq. is commonly used in TCM formulas and is recognized for its beneficial properties in treating conditions such as bronchitis, cough, pneumonia, lung injury and cancer, exhibiting pharmacological functions like expectorant, antitussive, antioxidant, anti-inflammatory and anticancer effects [14]. Curcumin, present in turmeric, demonstrates promising potential as an alternative therapy for LC with reduced side effects. Its anticancer effects in LC involve the regulation of various molecular targets, signaling

pathways, epigenetic changes, and microRNA expression [36]. *Astragalus membranaceus* improves quality of life and alleviates cancer symptoms in patients with metastatic diseases, including LC, by modulating the inflammatory cascade linked to in cytotoxic T lymphocytes, dendritic cells and macrophages in the initiation, metastasis, and progression of tumors [37]. Dihydroisotanshinone I (DT), extracted from the dried root of *Salvia miltiorrhiza*, demonstrates inhibitory effects on the growth of LC. Mechanistically, DT inhibits the expression of GPX4 and induces ferroptosis through lipid peroxidation [38]. *Matrine*, a natural active alkali in *S. flavescens*, shows therapeutic potential for non-small cell lung cancer by modulating reactive oxygen species-mediated autophagy and pyroptosis [39]. Additionally *Matrine* has been found to arrest the cell cycle between S phase and G2/M phase in non-small cell lung cancer, leading to tumor growth inhibition [40]. This study delves into the network diagram of drug-active ingredient-disease-common target relationships using network pharmacology. Key targets of FZQDP for LC treatment include STAT3, SRC, MAPK1, MAPK3, JUN, TP53, EGFR, MAPK14, TNF, and IL-6. Differentially expressed gene encoding subunits of STAT3, MAPK1, PRIM1, NADH, RAF1, MCM3 and JAK1 may play a role in the development of lung adenocarcinoma [41]. EGFR-mutant LCs exhibit genomic and clinical heterogeneity, with concurrent RB1/TP53 changes identifying a subset at higher risk for small cell transformation [42].

GO enrichment analysis indicated that the effects of FZQDP in LC are associated with various BP (e.g. negative modulation of vascular endothelial cell proliferation, IL-4 response, and DNA repair), CC (such as cyclin B1-CDK1 and IL-23 receptor complexes), and MF related to ubiquitination protein ligase binding and MAPK. KEGG enrichment analysis revealed that FZQDP primarily targets pathways in cancer, thyroid cancer, and regulation of lipolysis in adipocytes, suggesting its involvement in regulating multiple cancer pathways. In lung adenocarcinoma, ubiquitin-conjugating enzyme E2T has been shown to facilitate autophagy through the p53/AMPK/mTOR pathway [43]. Furthermore, numerous preclinical studies have highlighted the role of the PPAR pathway in modulating tumor progression by influencing various cellular processes such as apoptosis, proliferation, inflammation, angiogenesis, and metastasis in LC treatment [44]. Additionally, critical enzymes involved in arachidonic acid metabolism, including cyclooxygenase-2 and cytosolic phospholipase A2, have been implicated in the initiation, growth, and progression of various human malignancies, including LC [45,46].

Flow cytometry analysis confirmed that treatment with FZQDP or DDP can inhibit cell activity, promote cell apoptosis, and block the G2 phase compared to the control group. Similar effects have been observed in previous studies. For example, in the human LC cell line A549, curcumin and its derivatives have been shown to induce G2/M phase cell cycle arrest and p53-independent apoptosis [47]. Additionally, Tanshinone IIA from *S. miltiorrhiza* has been reported to cause G2/M phase arrest and activate the intrinsic apoptotic signaling pathway [48]. TCM has been noted for its minimal side effects and low toxicity, making it a promising option for alleviating the side effects of radiotherapy or chemotherapy in the treatment of LC [7,49]. These findings were further supported by a mouse tumor model in this study, where significant inhibition of tumor growth was observed without notable changes in body weight or spleen size.

Combined with network pharmacology analysis, JAK/STAT and MAPK signaling pathways target STAT3, MAPK3, and MAPK1. STAT3 plays a key role in regulating various cellular processes such as proliferation, survival, differentiation and immune response [50,51]. It is typically activated by external signaling molecules like cytokines and growth factors. The MAP kinase family members, MAPK3 and MAPK1, are involved in diverse cellular activities including differentiation, transcriptional control, and development. They play a significant role in regulating cell proliferation, cell cycle progression, apoptosis and cell differentiation [52]. IL-2 is predominantly secreted by $CD4^+$ T lymphocytes and acts on immune cells expressing IL-2 receptor (IL-2R) in an autocrine and paracrine manner. IL-2 activates various signaling pathways like JAK/STAT, MAPK, and PI3K-AKT, regulating the expression of genes that promote activation, growth, proliferation, differentiation, and activation-induced cell death (AICD) [53,54]. Stimulation with IL-2 is essential for maintaining regulatory T cells and for guiding the differentiation of $CD4^+$T cells into specific effector T cell subsets after antigen-mediated activation. In $CD8^+$ T cells, IL-2 signals play a critical role in enhancing the generation of effector T cells and facilitating their differentiation into memory cells [55]. Elevation of IL-2 activates the MAPK pathway, influencing cell proliferation, survival, and differentiation, as well as regulating immune cell function. Additionally, increase of levels of IL-2 promote $CD4^+$ T cell proliferation and activation, while also aiding in the regulation of different $CD4^+$ T cells subsets. IL-6 plays a crucial role in the JAK-STAT signaling pathway. Decreased IL-6 levels can inhibit the JAK-STAT pathway, impacting cell proliferation, differentiation, and immune response. IL-6 has been found to activate signaling pathways linked to tumor proliferation, particularly the JAK and STAT3 pathways. IL-6-induced JAK/STAT activation leads to constitutive STAT3 activation, associated with enhanced tumor cell growth and chemotherapy resistance [56]. IL-10 is capable of inhibiting Th1 cell differentiation and function [57]. Th1 cells are typically involved in cytotoxic immune responses and are crucial for anti-tumor immunity. Decreased IL-10 levels may reduce the inhibition of $CD4^+$ T cells, leading to their increased participation in the immune response. In conclusion, FZQDP has the potential to enhance immunity and inhibit tumor growth via the JAK/STAT and MAPK signaling pathways.

In terms of inhibiting tumor growth, both FZQDP and DDP treatments demonstrated inhibition of tumor growth, with DDP exhibiting stronger anti-tumor activity. However, DDP is associated with nephrotoxicity and hepatotoxicity, as evidenced by changes in circulating blood urea nitrogen, creatinine, and transaminases levels [58]. Analysis of blood biochemical indicators in this study revealed that levels of ALT, AST, BUN, and CRE in the FZQDF group were significantly lower compared to those in the DDP group, indicating lower liver and kidney toxicity in the FZQDF group. Additionally, H & E stained section analysis showed that liver and kidney damage in the FZQDP group was significantly lower than in the DDP group. Overall, toxicity observations suggest that FZQDF has fewer side effects and is safer. Moreover, FZQDF demonstrates positive effects on immune organs.

$CD4^+$ T cells are a specific subset of lymphocytes crucial in coordinating the immune response against diseases and infections [59]. The CD4/CD8 ratio, a hallmark of the collection of T cell defects related to aging known as “immunosenescence”, serves as a predictor of mortality in the general population [60]. Tumor growth often leads to immune evasion and overall immunosuppression, resulting in a decrease in effector T cells (CD4 and CD8) [61]. Our study suggests that treatment with FZQDP increased the $CD4^+$ T cell percentage

and $CD4^+/CD8^+$ ratio while reducing the $CD8^+$ T cell percentage in mouse spleen, indicating minimal harm to immune organs and a potential immune-boosting effect in mice. Similarly, administration of curcumin can prevent the depletion of central memory and effector memory T cells, potentially contributing to the rise in $CD4^+$ cells. Curcumin has demonstrated efficacy in restoring $CD4^+$ and $CD8^+$ T cell subsets, aiding in immune system recovery in cancer [61–63]. Polysaccharide extracted from *S. miltiorrhiza* can modulate immune function and enhance the host's innate immune response in higher vertebrates [64]. *A. membranaceus* polysaccharides are commonly utilized to enhance the immune systems of breast cancer patients [65]. TCM prescriptions containing *S. flavescens* have proven effective in treating ulcerative colitis by enhancing cell immunity, intestinal flora, and immune dysfunction in the intestinal mucosa [66]. An *in vivo* experiment illustrated that *F. thunbergii* has inhibitory effects on aberrant immune response by reducing inflammation and suppressing excessive prostate fibroblast proliferation [67]. However, further research is necessary to explore the mechanism of FZQDP in LC treatment.

This study has certain limitations that should be noted. The multi-target and multi-pathway characteristics of TCM prescriptions, such as FZQDP, suggest the potential for enhancing immunity and inhibiting tumor growth through the JAK/STAT and MAPK signaling pathways. Future experiments should focus on exploring the specific molecules of FZQDP and studying mechanisms and signaling pathways in depth. Additionally, due to the complexity of TCM prescriptions, it is important to identify the active ingredients in FZQDP that contribute to its anti-LC effects, offering new compounds for drug development. Furthermore, considering the holistic treatment approach of TCM, combining FZQDP with chemotherapy drugs like DDP, gemcitabine, paclitaxel, and pemetrexed could be beneficial. This combined treatment should be investigated to determine if FZQDP can enhance tumor response rates, prolong treatment duration, and potentially reduce toxicity while improving efficacy. Further research is needed to verify the impact on patient survival and the potential for reducing toxicity and increasing effectiveness.

## 5. Conclusion

This study investigated the potential active compounds of FZQDP in treating LC using network pharmacology. The research demonstrated that FZQDP could inhibit cell viability and enhance apoptosis through both *in vivo* and *in vitro* experiments. Additionally, FZQDP exhibited the ability to suppress tumor growth in mice by targeting LC cells and enhancing immune function. Furthermore, as a TCM used in clinical practice, FZQDP showed minimal toxicity. Overall, FZQDP presents itself as a promising treatment option of LC, potentially serving as an effective adjuvant therapy.

## Funding

Funding for this research was partially provided by grants from the National Natural Science Foundation of China (No. 82004179) and the Fundamental Research Funds for the Central Public Welfare Research Institutes (No. ZZ14-YQ-013).

## Consent for publication

Not applicable.

## Data availability statement

The data supporting the findings of this study can be obtained from the corresponding author upon request.

## Submission declaration and verification

The work presented in this study has not been previously published, is not being considered for publication elsewhere, has been approved for publication by all authors and the relevant authorities, and will not be published in any other form without consent.

## Ethics approval

All animal experiments were conducted in compliance with ethical standards and were approved by the ethics committee of the Guang'anmen Hospital, China Academy of Chinese Medical Sciences (Approval No. 2020-011-SQ), following national guidelines for animal experimentation.

## CRediT authorship contribution statement

**Binjie Su:** Writing – review & editing, Writing – original draft, Visualization, Validation, Supervision, Software, Resources, Project administration, Methodology, Investigation, Formal analysis, Data curation, Conceptualization. **Qiyuan Mao:** Writing – review & editing, Writing – original draft, Visualization, Validation, Resources, Methodology, Investigation, Formal analysis, Conceptualization. **Daorui Li:** Writing – review & editing, Writing – original draft, Visualization, Validation, Funding acquisition, Formal analysis, Data curation. **Yingyi Wu:** Writing – review & editing, Writing – original draft, Visualization, Resources, Methodology, Data curation. **Bo Wang:** Writing – review & editing, Writing – original draft, Visualization, Validation, Investigation, Formal analysis, Data curation. **Xueqian Wang:** Writing – review & editing, Supervision, Project administration, Funding acquisition, Conceptualization.

## Declaration of competing interest

The authors declare that they have no known competing financial interests or personal relationships that could have appeared to influence the work reported in this paper.

## Acknowledgement

Not applicable.

## Appendix A. Supplementary data

Supplementary data to this article can be found online at https://doi.org/10.1016/j.heliyon.2024.e37546.

## References

[1] M.B. Schabath, M.L. Cote, Cancer progress and priorities: lung cancer, Cancer Epidemiol. Biomarkers Prev. 28 (2019) 1563–1579.
[2] F. Bray, M. Laversanne, H. Sung, J. Ferlay, R.L. Siegel, I. Soerjomataram, A. Jemal, Global cancer statistics 2022: GLOBOCAN estimates of incidence and mortality worldwide for 36 cancers in 185 countries, CA Cancer J Clin 74 (3) (2024) 229–263.
[3] F. Nasim, B.F. Sabath, G.A. Eapen, Lung cancer, Med. Clin. 103 (2019) 463–473.
[4] X.L. Su, J.W. Wang, H. Che, C.F. Wang, H. Jiang, X. Lei, W. Zhao, H.X. Kuang, Q.H. Wang, Clinical application and mechanism of traditional Chinese medicine in treatment of lung cancer, Chin Med J (Engl) 133 (2020) 2987–2997.
[5] Z. Li, Z. Feiyue, L. Gaofeng, Traditional Chinese medicine and lung cancer–From theory to practice, Biomed. Pharmacother. 137 (2021) 111381.
[6] E. Sun, X. Meng, Z. Kang, H. Gu, M. Li, X. Tan, L. Feng, X. Jia, Zengshengping improves lung cancer by regulating the intestinal barrier and intestinal microbiota, Front. Pharmacol. 14 (2023) 1123819.
[7] Y. Xiang, Z. Guo, P. Zhu, J. Chen, Y. Huang, Traditional Chinese medicine as a cancer treatment: modern perspectives of ancient but advanced science, Cancer Med. 8 (2019) 1958–1975.
[8] S. Huang, Y. Chen, L. Pan, C. Fei, N. Wang, F. Chu, D. Peng, X. Duan, Y. Wang, Exploration of the potential mechanism of tao hong Si Wu decoction for the treatment of breast cancer based on network pharmacology and in vitro experimental verification, Front. Oncol. 11 (2021) 731522.
[9] P. Chen, Q. Wu, J. Feng, L. Yan, Y. Sun, S. Liu, Y. Xiang, M. Zhang, T. Pan, X. Chen, T. Duan, L. Zhai, B. Zhai, W. Wang, R. Zhang, B. Chen, X. Han, Y. Li, L. Chen, Y. Liu, X. Huang, T. Jin, W. Zhang, H. Luo, X. Chen, Y. Li, Q. Li, G. Li, Q. Zhang, L. Zhuo, Z. Yang, H. Tang, T. Xie, X. Ouyang, X. Sui, Erianin, a novel dibenzyl compound in Dendrobium extract, inhibits lung cancer cell growth and migration via calcium/calmodulin-dependent ferroptosis, Signal Transduct Target Ther 5 (2020) 51.
[10] M. Kanai, K. Yoshimura, M. Asada, A. Imaizumi, C. Suzuki, S. Matsumoto, T. Nishimura, Y. Mori, T. Masui, Y. Kawaguchi, K. Yanagihara, S. Yazumi, T. Chiba, S. Guha, B.B. Aggarwal, A phase I/II study of gemcitabine-based chemotherapy plus curcumin for patients with gemcitabine-resistant pancreatic cancer, Cancer Chemother. Pharmacol. 68 (2011) 157–164.
[11] Y. Tan, X. Wei, W. Zhang, X. Wang, K. Wang, B. Du, J. Xiao, Resveratrol enhances the radiosensitivity of nasopharyngeal carcinoma cells by downregulating E2F1, Oncol. Rep. 37 (2017) 1833–1841.
[12] Z. Li, J. Qi, T. Guo, J. Li, Research progress of Astragalus membranaceus in treating peritoneal metastatic cancer, J. Ethnopharmacol. 305 (2023) 116086.
[13] W. Zhang, C. Liu, J. Li, Y. Lu, H. Li, J. Zhuang, X. Ren, M. Wang, C. Sun, Tanshinone IIA: new perspective on the anti-tumor mechanism of A traditional natural medicine, Am. J. Chin. Med. 50 (2022) 209–239.
[14] F. Wu, M. Tian, Y. Sun, C. Wu, X. Liu, Efficacy, chemical composition, and pharmacological effects of herbal drugs derived from Fritillaria cirrhosa D. Don and Fritillaria thunbergii Miq, Front. Pharmacol. 13 (2022) 985935.
[15] Q. He, C. Liu, X. Wang, K. Rong, M. Zhu, L. Duan, P. Zheng, Y. Mi, Exploring the mechanism of curcumin in the treatment of colon cancer based on network pharmacology and molecular docking, Front. Pharmacol. 14 (2023) 1102581.
[16] M.H. Chen, Y.Y. Gu, A.L. Zhang, D.M. Sze, S.L. Mo, B.H. May, Biological effects and mechanisms of matrine and other constituents of Sophora flavescens in colorectal cancer, Pharmacol. Res. 171 (2021) 105778.
[17] F. Yan, X. Wang, Y. Xie, X. Liu, L. Yu, P. Wang, T. Li, S. Wang, W. Li, Z. Yang, Yangyin Fuzheng Jiedu Prescription exerts anti-tumor immunity in hepatocellular carcinoma by alleviating exhausted T cells, Phytomedicine 91 (2021) 153722.
[18] A.G. Zhou, D.W. Huang, Y.X. Ding, H. Jiang, M.L. Tang, Treatment of postoperative gastric cancer with the Fuzheng Huoxue anticancer prescription, World J. Gastroenterol. 3 (1997) 189–191.
[19] Y. Xie, F. Yan, X. Wang, L. Yu, H. Yan, Q. Pu, W. Li, Z. Yang, Mechanisms and network pharmacological analysis of Yangyin Fuzheng Jiedu prescription in the treatment of hepatocellular carcinoma, Cancer Med. 12 (2023) 3237–3259.
[20] X. Li, H. Yu, Y. Gong, P. Wu, Q. Feng, C. Liu, Fuzheng Xiaozheng prescription relieves rat hepatocellular carcinoma through improving anti-inflammation capacity and regulating lipid related metabolisms, J. Ethnopharmacol. 284 (2022) 114801.
[21] L. Shang, Y. Wang, J. Li, F. Zhou, K. Xiao, Y. Liu, M. Zhang, S. Wang, S. Yang, Mechanism of Sijunzi Decoction in the treatment of colorectal cancer based on network pharmacology and experimental validation, J. Ethnopharmacol. 302 (2023) 115876.
[22] T. Kohno, T. Sato, S. Takakura, K. Takei, K. Inoue, M. Nishioka, J. Yokota, Mutation and expression of the DCC gene in human lung cancer, Neoplasia 2 (2000) 300–305.
[23] M. Tani, K. Shimizu, C. Kawahara, T. Kohno, O. Ishimoto, S. Ikawa, J. Yokota, Mutation and expression of the p51 gene in human lung cancer, Neoplasia 1 (1999) 71–79.
[24] K. Inamura, Lung cancer: understanding its molecular pathology and the 2015 WHO classification, Front. Oncol. 7 (2017) 193.
[25] Z. Liu, Q. Shang, H. Li, D. Fang, Z. Li, Y. Huang, M. Zhang, K.M. Ko, J. Chen, Exploring the possible mechanism(s) underlying the nephroprotective effect of Zhenwu Decoction in diabetic kidney disease: an integrated analysis, Phytomedicine 119 (2023) 154988.
[26] A. Daina, O. Michielin, V. Zoete, SwissTargetPrediction: updated data and new features for efficient prediction of protein targets of small molecules, Nucleic Acids Res. 47 (2019) W357–w364.
[27] L. Fu, L. Zhao, F. Li, F. Wen, P. Zhang, X. Yang, Y. Wang, Pharmacological mechanism of quercetin in the treatment of colorectal cancer by network pharmacology and molecular simulation, J. Biomol. Struct. Dyn. (2023) 1–12.
[28] F. Yang, Y. Gu, Y. Yan, G. Wang, Based on network pharmacology and molecular docking to predict the mechanism of TMDZ capsule in the treatment of IS, Medicine (Baltim.) 102 (2023) e34424.
[29] L. Zhao, X. Zhu, Y. Ni, J. You, A. Li, Xiaoyaosan, a traditional Chinese medicine, inhibits the chronic restraint stress-induced liver metastasis of colon cancer in vivo, Pharm. Biol. 58 (2020) 1085–1091.

[30] Q. Man, Y. Deng, P.J. Li, J. Ma, Z.J. Yang, X.J. Yang, Y. Zhou, X. Yan, Licorice ameliorates cisplatin-induced hepatotoxicity through antiapoptosis, antioxidative stress, anti-inflammation, and acceleration of metabolism, Front. Pharmacol. 11 (2020).
[31] Q. Ren, F. Guo, S.B. Tao, R.S. Huang, L. Ma, P. Fu, Flavonoid fisetin alleviates kidney inflammation and apoptosis via inhibiting Src-mediated NF-κB p65 and MAPK signaling pathways in septic AKI mice, Biomed. Pharmacother. 122 (2020).
[32] R. Salehi-Rad, R. Li, M.K. Paul, S.M. Dubinett, B. Liu, The biology of lung cancer: development of more effective methods for prevention, diagnosis, and treatment, Clin. Chest Med. 41 (2020) 25–38.
[33] B.C. Bade, C.S. Dela Cruz, Lung cancer 2020: epidemiology, etiology, and prevention, Clin. Chest Med. 41 (2020) 1–24.
[34] X.R. He, S.Y. Han, P.P. Li, Recent highlights of Chinese medicine for advanced lung cancer, Chin. J. Integr. Med. 23 (2017) 323–330.
[35] H. Nie, Z. Han, S. Nicholas, E. Maitland, Z. Huang, S. Chen, Z. Tuo, Y. Ma, X. Shi, Costs of traditional Chinese medicine treatment for inpatients with lung cancer in China: a national study, BMC Complement Med Ther 23 (2023) 5.
[36] W.N.B. Wan Mohd Tajuddin, N.H. Lajis, F. Abas, I. Othman, R. Naidu, Mechanistic understanding of curcumin's therapeutic effects in lung cancer, Nutrients 11 (2019).
[37] O.A. Bamodu, K.T. Kuo, C.H. Wang, W.C. Huang, A.T.H. Wu, J.T. Tsai, K.Y. Lee, C.T. Yeh, L.S. Wang, Astragalus polysaccharides (PG2) enhances the M1 polarization of macrophages, functional maturation of dendritic cells, and T cell-mediated anticancer immune responses in patients with lung cancer, Nutrients 11 (2019).
[38] C.Y. Wu, Y.H. Yang, Y.S. Lin, G.H. Chang, M.S. Tsai, C.M. Hsu, R.A. Yeh, L.H. Shu, Y.C. Cheng, H.T. Liu, Dihydroisotanshinone I induced ferroptosis and apoptosis of lung cancer cells, Biomed. Pharmacother. 139 (2021) 111585.
[39] D. Luo, X. Dai, H. Tian, C. Fan, H. Xie, N. Chen, J. Wang, L. Huang, H. Wang, G. Wang, Y. Zhang, Sophflarine A, a novel matrine-derived alkaloid from Sophora flavescens with therapeutic potential for non-small cell lung cancer through ROS-mediated pyroptosis and autophagy, Phytomedicine 116 (2023) 154909.
[40] Q. An, C. Han, Y. Zhou, F. Li, D. Li, X. Zhang, Z. Yu, Z. Duan, Q. Kan, Matrine induces cell cycle arrest and apoptosis with recovery of the expression of miR-126 in the A549 non-small cell lung cancer cell line, Mol. Med. Rep. 14 (2016) 4042–4048.
[41] H. Xu, J. Ma, J. Wu, L. Chen, F. Sun, C. Qu, D. Zheng, S. Xu, Gene expression profiling analysis of lung adenocarcinoma, Braz. J. Med. Biol. Res. 49 (2016).
[42] M. Offin, J.M. Chan, M. Tenet, H.A. Rizvi, R. Shen, G.J. Riely, N. Rekhtman, Y. Daneshbod, A. Quintanal-Villalonga, A. Penson, M.D. Hellmann, M.E. Arcila, M. Ladanyi, D. Pe'er, M.G. Kris, C.M. Rudin, H.A. Yu, Concurrent RB1 and TP53 alterations define a subset of EGFR-mutant lung cancers at risk for histologic transformation and inferior clinical outcomes, J. Thorac. Oncol. 14 (2019) 1784–1793.
[43] J. Zhu, H. Ao, M. Liu, K. Cao, J. Ma, UBE2T promotes autophagy via the p53/AMPK/mTOR signaling pathway in lung adenocarcinoma, J. Transl. Med. 19 (2021) 374.
[44] A.K. Reka, M.T. Goswami, R. Krishnapuram, T.J. Standiford, V.G. Keshamouni, Molecular cross-regulation between PPAR-gamma and other signaling pathways: implications for lung cancer therapy, Lung Cancer 72 (2011) 154–159.
[45] C. Li, Z. Wang, W. Chen, B. Cao, M. Zhang, Q. Gu, S. Qi, X. Fei, Y. Shi, X. Li, R. Li, J. Wang, G. Li, An integrative metabolomic and network pharmacology study revealing the regulating properties of xihuang pill that improves anlotinib effects in lung cancer, Front. Oncol. 11 (2021) 697247.
[46] H. Ling, X. Jia, Y. Zhang, L.A. Gapter, Y.S. Lim, R. Agarwal, K.Y. Ng, Pachymic acid inhibits cell growth and modulates arachidonic acid metabolism in nonsmall cell lung cancer A549 cells, Mol. Carcinog. 49 (2010) 271–282.
[47] N. Namwan, G. Senawong, C. Phaosiri, P. Kumboonma, L.O. Somsakeesit, A. Samankul, C. Leerat, T. Senawong, HDAC inhibitory and anti-cancer activities of curcumin and curcumin derivative CU17 against human lung cancer A549 cells, Molecules 27 (2022).
[48] J. Chen, D.Y. Shi, S.L. Liu, L. Zhong, Tanshinone IIA induces growth inhibition and apoptosis in gastric cancer in vitro and in vivo, Oncol. Rep. 27 (2012) 523–528.
[49] F. Yan, M. Feng, X. Wang, P. Wang, Y. Xie, X. Liu, W. Li, Z. Yang, Molecular targets of Yangyin Fuzheng Jiedu Prescription in the treatment of hepatocellular carcinoma based on network pharmacology analysis, Cancer Cell Int. 20 (2020) 540.
[50] J.S. Rawlings, K.M. Rosler, D.A. Harrison, The JAK/STAT signaling pathway, J. Cell Sci. 117 (2004) 1281–1283.
[51] S. Zou, Q. Tong, B. Liu, W. Huang, Y. Tian, X. Fu, Targeting STAT3 in cancer immunotherapy, Mol. Cancer 19 (2020) 145.
[52] Y.J. Guo, W.W. Pan, S.B. Liu, Z.F. Shen, Y. Xu, L.L. Hu, ERK/MAPK signalling pathway and tumorigenesis, Exp. Ther. Med. 19 (2020) 1997–2007.
[53] B.H. Nelson, J.D. Lord, P.D. Greenberg, Cytoplasmic domains of the interleukin-2 receptor beta and gamma chains mediate the signal for T-cell proliferation, Nature 369 (1994) 333–336.
[54] H.P. Kim, J. Imbert, W.J. Leonard, Both integrated and differential regulation of components of the IL-2/IL-2 receptor system, Cytokine Growth Factor Rev. 17 (2006) 349–366.
[55] O. Boyman, J. Sprent, The role of interleukin-2 during homeostasis and activation of the immune system, Nat. Rev. Immunol. 12 (2012) 180–190.
[56] L. Browning, M.R. Patel, E.B. Horvath, K. Tawara, C.L. Jorcyk, IL-6 and ovarian cancer: inflammatory cytokines in promotion of metastasis, Cancer Manag. Res. 10 (2018) 6685–6693.
[57] C.L. Maynard, C.T. Weaver, Diversity in the contribution of interleukin-10 to T-cell-mediated immune regulation, Immunol. Rev. 226 (2008) 219–233.
[58] S. Ghosh, Cisplatin: the first metal based anticancer drug, Bioorg. Chem. 88 (2019) 102925.
[59] S.L. Swain, K.K. McKinstry, T.M. Strutt, Expanding roles for CD4(+) T cells in immunity to viruses, Nat. Rev. Immunol. 12 (2012) 136–148.
[60] S. Serrano-Villar, T. Sainz, S.A. Lee, P.W. Hunt, E. Sinclair, B.L. Shacklett, A.L. Ferre, T.L. Hayes, M. Somsouk, P.Y. Hsue, M.L. Van Natta, C.L. Meinert, M. M. Lederman, H. Hatano, V. Jain, Y. Huang, F.M. Hecht, J.N. Martin, J.M. McCune, S. Moreno, S.G. Deeks, HIV-infected individuals with low CD4/CD8 ratio despite effective antiretroviral therapy exhibit altered T cell subsets, heightened CD8+ T cell activation, and increased risk of non-AIDS morbidity and mortality, PLoS Pathog. 10 (2014) e1004078.
[61] S. Bose, A.K. Panda, S. Mukherjee, G. Sa, Curcumin and tumor immune-editing: resurrecting the immune system, Cell Div. 10 (2015) 6.
[62] S. Paul, G. Sa, Curcumin as an adjuvant to cancer immunotherapy, Front. Oncol. 11 (2021) 675923.
[63] S. Bhattacharyya, D. Md Sakib Hossain, S. Mohanty, G. Sankar Sen, S. Chattopadhyay, S. Banerjee, J. Chakraborty, K. Das, D. Sarkar, T. Das, G. Sa, Curcumin reverses T cell-mediated adaptive immune dysfunctions in tumor-bearing hosts, Cell. Mol. Immunol. 7 (2010) 306–315.
[64] D. Chen, L. Yang, F. Yang, Q. Pei, L. Lu, X. Huang, P. Ouyang, Y. Geng, Z. Li, X. Zhang, J. Wang, D. Chen, Salvia miltiorrhiza polysaccharide activated macrophages and improved the disease resistance of sturgeon against Aeromonas hydrophila, Fish Shellfish Immunol. 127 (2022) 594–603.
[65] L. Zhou, Z. Liu, Z. Wang, S. Yu, T. Long, X. Zhou, Y. Bao, Astragalus polysaccharides exerts immunomodulatory effects via TLR4-mediated MyD88-dependent signaling pathway in vitro and in vivo, Sci. Rep. 7 (2017) 44822.
[66] M. Chen, Y. Ding, Z. Tong, Efficacy and safety of Sophora flavescens (kushen) based traditional Chinese medicine in the treatment of ulcerative colitis: clinical evidence and potential mechanisms, Front. Pharmacol. 11 (2020) 603476.
[67] J. Mastio, T. Condamine, G. Dominguez, A.V. Kossenkov, L. Donthireddy, F. Veglia, C. Lin, F. Wang, S.Y. Fu, J. Zhou, P. Viatour, S. Lavilla-Alonso, A.T. Polo, E. N. Tcyganov, C. Mulligan, B. Nam, J. Bennett, G. Masters, M. Guarino, A. Kumar, Y. Nefedova, R.H. Vonderheide, L.R. Languino, S.I. Abrams, D.I. Gabrilovich, Identification of monocyte-like precursors of granulocytes in cancer as a mechanism for accumulation of PMN-MDSCs, J. Exp. Med. 216 (2019) 2150–2169.